JRSR 7 (2020) 134-140

Journal of Rehabilitation Sciences and Research

Journal Home Page: jrsr.sums.ac.ir

Original Article

Numerical Simulation of the Early Stages of Glaucoma in Human Eye

Ali Reza Tahavvor*, PhD; Mohsen Gholami, MSc

Department of Mechanical Engineering, Shiraz Branch, Islamic Azad University, Shiraz, Iran

ARTICLE INFO

Article History:
Received: 25/06/2019
Revised: 25/08/2020
Accepted: 02/09/2020

Keywords:
Human eye
Glaucoma
Retina
Eye pressure
Fluid-structure

Please cite this article as:
Tahavvor AR, Gholami M. Numerical Simulation of the Early Stages of Glaucoma in Human Eye. JRSR. 2020;7(3):134-140.

ABSTRACT

Background: The eye is one of the most vital organs of human body, and glaucoma is the second-leading cause of blindness after cataracts in the world. However, glaucoma is the leading cause of preventable blindness. The main objective of this study is to investigate intraocular pressure (IOP), stress, strain, and deformation in the retina in early stages of glaucoma.

Methods: In this study, a model of the human eye is numerically investigated. The aqueous humor pressure is considered as 30, 35, and 40 mmHg and compared with normal eye pressure. The problem is considered as transient 3D and accurate. Comparison between obtained results shows that the model has been applied. Eye components are also considered with their real properties. Due to the inappreciable effects of turbulence and temperature variation, these effects have been neglected. To determine the pressure field, a two-way fluid-structure interaction is applied, and then, the results are used in a one-way fluid-structure interaction to determine the amount of stress, strain, and deformation of the retina.

Results: The maximum deformation in the retina of a glaucoma patient is about 0.33 mm higher than a normal eye, the maximum stress is about 1,300 Pa higher than a normal eye, and the maximum strain is about 0.06 higher than a normal eye.

Conclusion: In patients with increased IOP, the amount of deformation in the retina has increased, and the maximum deformation occurs near the optic disc in all cases. Furthermore, maximum stress and maximum strain occur at the place of maximum deformation.

2020© The Authors. Published by JRSR. All rights reserved.

Introduction

The eye is one of the most vital parts of the human body, and sight plays an important role in every person's life. The size of the human adult eye is about 22 to 24.8 mm (axial) x 24.2 mm (horizontal) x 23.7 mm (vertical) [1]. The eye layer is composed of sclera, choroid, and retina. The sclera in the front turns into the cornea, so light can pass through it. The choroid is converted to the iris (the colored part of the eye) in the front to control the amount of incoming light. Unlike the choroid, the iris is flat. In fact, light passes through the middle hole of the iris known as the pupil. The lens is a transparent part behind the iris. Actually, the lens plays the greatest role in refraction. The retina is the inner layer of the eye. The average retina thickness is 0.235 mm [2]. This layer is composed of the optic nerve. The images of objects are reflected on it, then transmitted to the brain. In the rear of the retina, there is a blind spot where known as the optic disc where there are no photoreceptors. This area is very important and sensitive.

Glaucoma is an eye disease that can permanently damage vision and even lead to blindness. It is a preventable disease, so studying it is important. In most cases, glaucoma is directly related to intraocular pressure (IOP). Aqueous humor (AH) flows in the front of the eye

*Corresponding author: Ali Reza Tahavvor, Department of Mechanical Engineering, Shiraz Branch, Islamic Azad University, P.O. Box 71993-5, Shiraz, Iran. **Tel:** +98 9173154695;
Email: tahavvor@iaushiraz.ac.ir

to feed the lens and cornea. If AH can't leave the eye or its drainage is reduced, then IOP is increased. The increased pressure is transferred to the vitreous humor (VH) in the posterior section of the eye and causes damage to the retina. VH pressure on the optic disc causes stress in this area and loss of vision over time. The damage to the optic disc is irreversible. This process is called glaucoma. The components of the eye are illustrated in Figure 1-a.

Visualization of the aqueous outflow pathway in glaucoma surgery was studied by Broquet et al. [3]. Akhmanova et al. researched hydraulic flows and the transport of drugs in the human eye [4]. Exposure of the human eye to wind with a simple eye model has also been studied [5]. Heys and Barocas studied natural convection in AH in glaucoma disease with a simple model [6]. Heat transfer in the human eye using the finite element method was researched by Cicekli in his thesis [7] as well as in other studies [8-10]. The influence of the geometry of the sclera on optic nerve head biomechanics and connections with glaucoma has been studied by Norman et al. [11]. Optic nerve head biomechanics was studied by Sigal et al. with the finite element method [12]. This issue was further studied by Wang et al. in an experimental research [13]. In fact, the analysis of this area is very important because of its sensitivity to glaucoma disease. The purpose of the current study is to investigate the early stages of glaucoma in the human eye and identify changes in the optic disc. The present study is innovative in terms of the exact model and use of the fluid-structure interaction technique.

Methods

In this study, the transient 3D model of the human eye with exact dimensions was simulated to obtain the amount of stress, strain, and deformation in the retina. This model contains all the main components of the eye and all components needed for analysis. The model is shown in Figure 1-b.

For this research, the computational fluid dynamics and structural analysis approaches based on the finite volume and finite element methods were used, respectively. Governing equations for fluid/solid media are presented below.

Fluid Flow Equations

The fluid equations to be solved are the incompressible Navier-Stokes equations, which can be derived from the conservation laws for mass and linear momentum and take into consideration that the fluid is viscous. The equations take the following form:

$$\rho^F \frac{dv}{dt} + \rho^F \cdot c \cdot \nabla v - 2\mu\nabla \cdot \varepsilon(v) + \nabla p = 0 \quad (1)$$

$$\nabla \cdot v = 0$$

where v denotes fluid velocity and p denotes physical pressure. The fluid density and viscosity is given by ρ^F and μ, respectively, $(\boldsymbol{v})$ represents the strain rate tensor, and c denotes convective velocity and is defined as follows:

$$c = v\text{-}v^* \quad (2)$$

where v and v^* are the material and mesh velocity, respectively.

Structural Equation

The possibly large displacement of the structure is governed by:

$$\rho^s \frac{D^2 u}{Dt^2} - \nabla \cdot (F \cdot S(u)) = \rho^s b^s \quad (3)$$

where u represents the displacements of the structure, $\boldsymbol{b}^s$ represents the body forces applied on the structure, S represents the stress tensor, ρ^s represents the density of the structure, and F represents the deformation gradient tensor.

Fluid/Solid Coupling Equations

At the interface Γ, kinematic and dynamic continuity is required. The governing kinematic coupling equations are:

$$u_\Gamma(t) = d_\Gamma^F(t) \quad (4)$$

$$\dot{u}_\Gamma(t) = v_\Gamma(t)$$

$$\ddot{u}_\Gamma(t) = \dot{v}_\Gamma(t)$$

Here $d_\Gamma^F(t)$ represents the displacement of the fluid mesh nodes at the interface. The dynamic coupling equation takes the form:

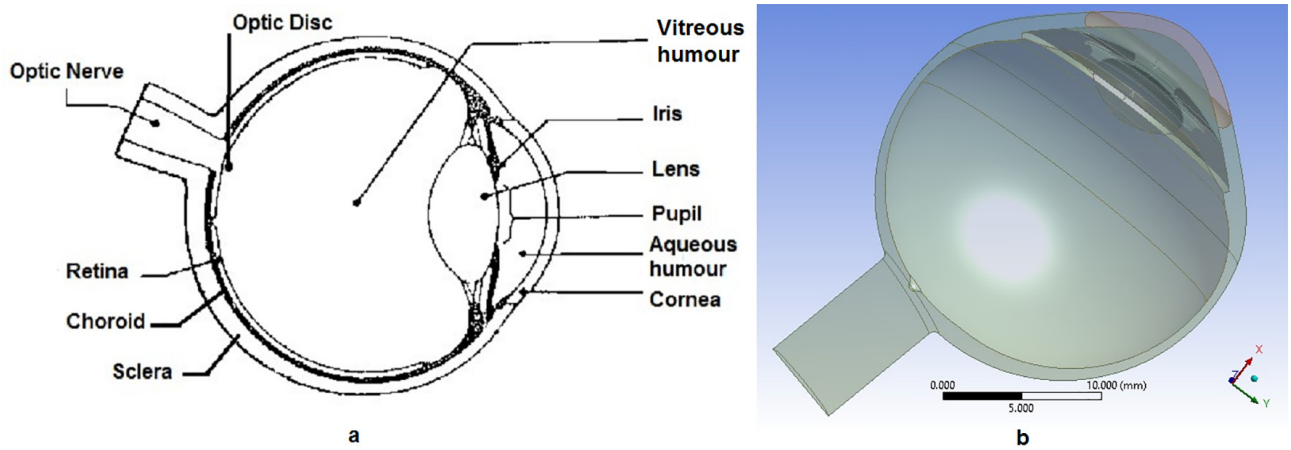

Figure 1-a: Human eye components, **b:** Three-dimensional model of the eye

$$h^S(t) + h^F(t) = 0 \quad (5)$$

where $\boldsymbol{h} = \boldsymbol{\sigma} \cdot \boldsymbol{n}$ signifies the traction vector.

The maximum IOP for the normal eye is approximately 22 mm Hg [14]. The amounts of stress, strain, and deformation in the retina for the pressures of 30, 35, and 40 mmHg in AH are calculated and the results compared with 22 mmHg as the maximum normal eye pressure. In glaucoma, the AH remains stagnant in the front section of the eye, and there is no entry or exit; thus, a normal pressure on the surface in that area of the eye instead of liquid pressure is assumed (Figure 2).

Therefore, the porosity of the ciliary body and the trabecular meshwork, which are the locations of the entrance and exit of AH, respectively, is not affected in the present work. This effect has been studied previously [3, 10, 15]. Also, the difference in temperature in the anterior section of the eye that causes free convection in the AH is not considered. As mentioned, the effect of temperature has been extensively studied. The fluid-structure interaction (FSI) technique was used for simulation. FSI between the solid parts (lens, iris etc.) and the VH is two-way, and FSI between the VH and the retina is one-way, as shown in Figure 3.

First, two-way FSI was applied and the pressure values for the VH were obtained. Then, two-way FSI solution was used as a one-way FSI input, and the stress, strain, and deformation values in the retina were obtained.

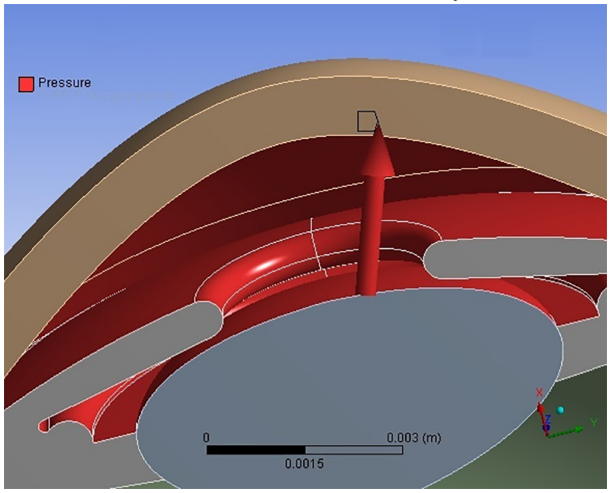

Figure 2. Normal pressure on the surfaces

According to the type of geometry, an unstructured grid was used. Therefore, the type of grid cells chosen for all modules was hexagonal. To achieve grid independent solution, several grid sizes were used. Comparison of the obtained results from various grid sizes, as indicated in Table 1, showed that the 441,448 elements were of a suitable grid size. This number is 198,166 and 8184 for solid analysis in the two-way FSI and one-way FSI, respectively. Different grids are shown in Figure 4.

Due to the low-velocity fluids, the effect of the turbulence was negligible. Moreover, eye components were considered with their real properties. The properties of fluids and solids are shown in Tables 2 and 3, respectively.

Table 1: Grid study results

Number of elements	Minimum strain in optic disc
219,734	3.22 %
294,298	3.37 %
441,448	3.61%
663,182	3.60%

Table 2: Fluid Properties

Name	Density (g/cm^3)	Viscosity (cP)
Vitreous Humor	1.002 [16]	1000 [17]

Results and Discussion

The contours of deformation for different pressures were obtained after solving (Figure 5).

These contours show that the maximum deformation in all cases is near the optic disc. The maximum retina deformation in the normal eye is 0.14795 mm. The maximum retina deformation at IOP of 30 mmHg is 0.17746 mm, which is 0.02951 mm higher than the normal eye (19/94% increased deformation). The maximum retina deformation at IOP of 35 mmHg is 0.17753 mm, which is 0.02958 mm higher than the normal eye (19.99% increased deformation), and the maximum retina deformation at IOP of 40 mmHg is 0.17754 mm, which is 0.02959 mm higher than the

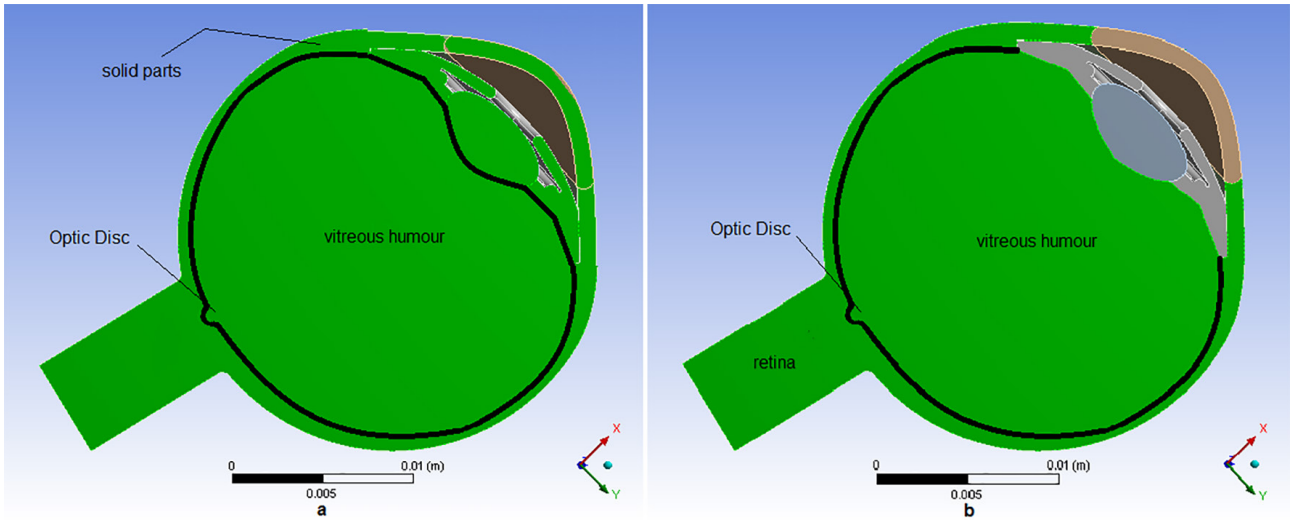

Figure 3–a: Two-way fluid structure interaction (FSI) between the solid parts and Vitreous humor (VH); **b:** One-way FSI between VH and retina

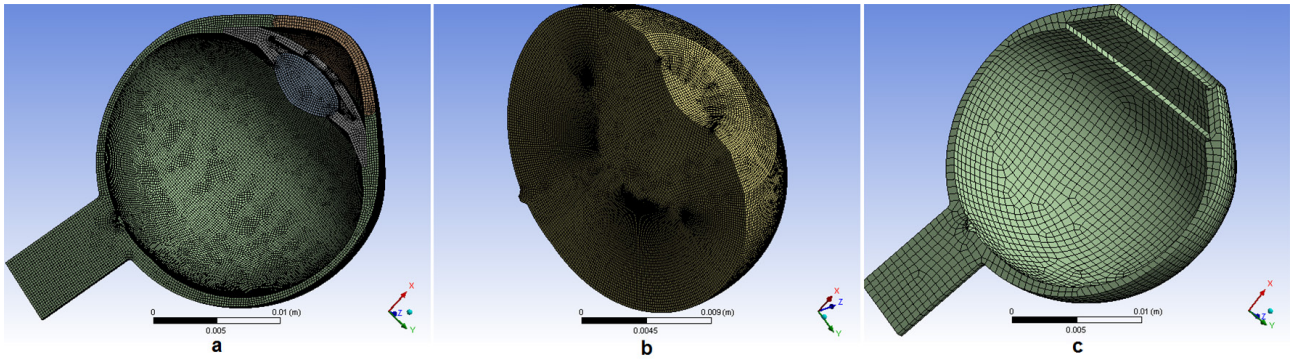

Figure 4-a: Grid for analysis in two-way FSI; **b:** Grid for fluid analysis in both FSIs; **c:** Grid for analysis in one-way FSI

Table 3: Solid Properties

Names	Density (g/cm^3)	Young's Modulus (KPa)	Poisson's Ratio
Sclera	1.049 [16]	2720 [18]	0.49 [19]
Choroid	1.002 [16]	600 [20]	0.49 [19]
Retina	1.008 [16]	20 [21]	0.47 [22]
Iris	1.1 [8]	890 [23]	0.48 [23]
Lens	1.056 [16]	1.5 [24]	0.49 [25]
Cornea	1.024 [16]	2500 [18]	0.2 [26]
Average of Sclera, Choroid, and Retina	1.049	2300 [20]	0.49

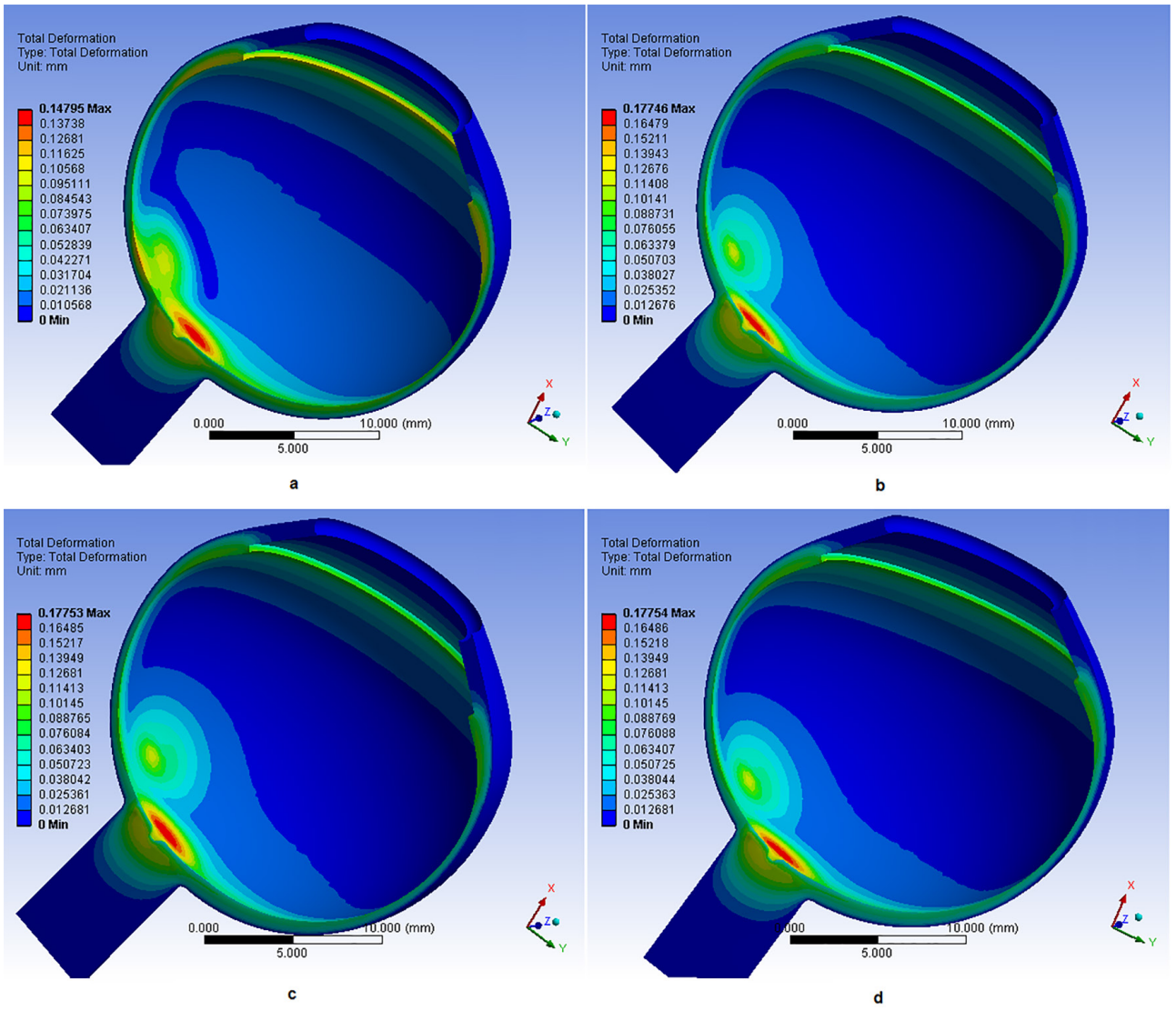

Figure 5–a: Contours of deformation in the retina for 22 mmHg of intraocular pressure (IOP) (as a normal eye); **b:** Contours of deformation in the retina for 30 mmHg of IOP; **c:** Contours of deformation in the retina for 35 mmHg of IOP; **d:** Contours of deformation in the retina for 40 mmHg of IOP

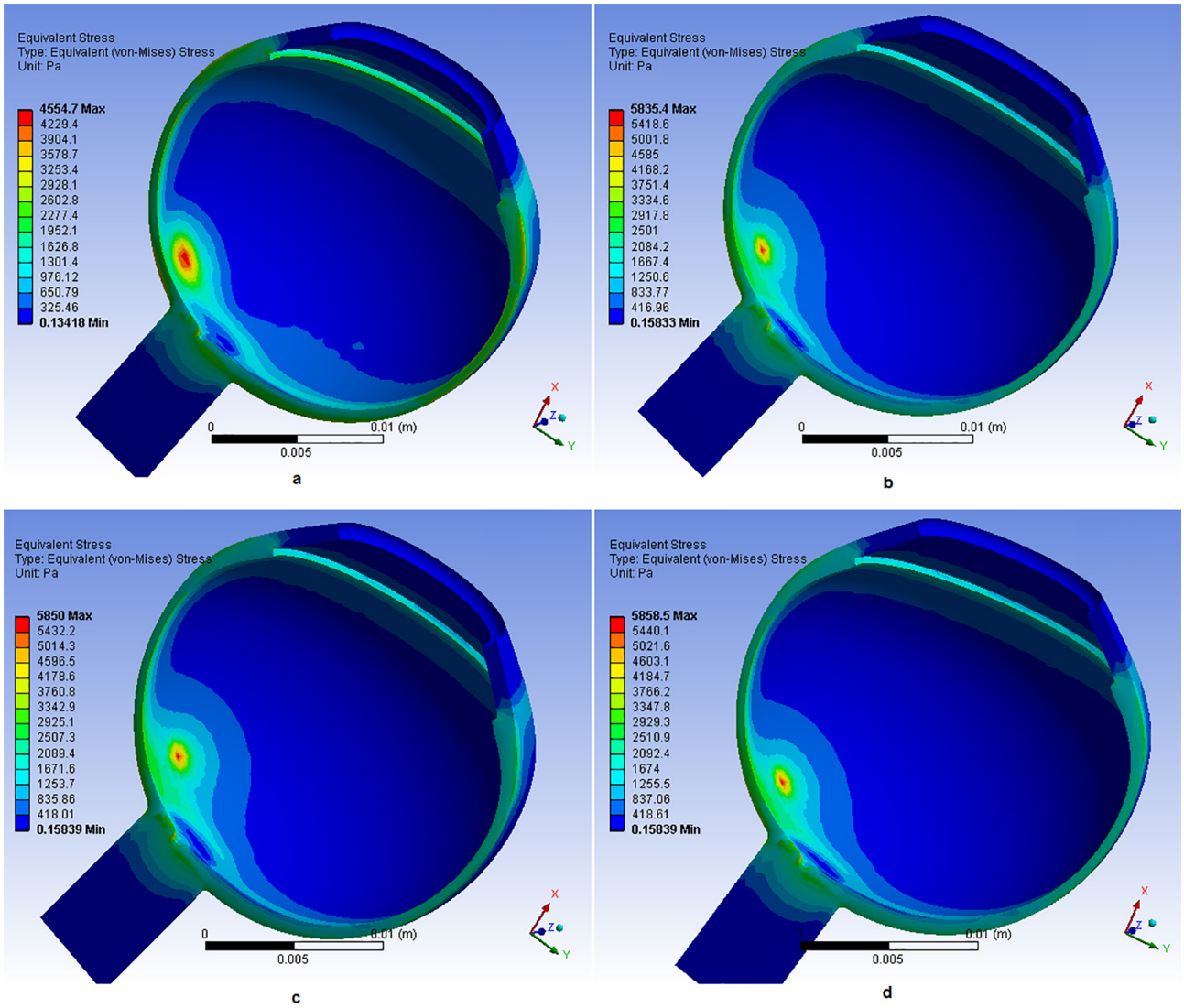

Figure 6-a: Contours of stress in the retina for 22 mmHg of IOP (as a normal eye); **b:** Contours of stress in the retina for 30 mmHg of IOP; **c:** Contours of stress in the retina for 35 mmHg of IOP; **d:** Contours of stress in the retina for 40 mmHg of IOP

Table 4: Comparison of maximum deformation, stress, and strain in the retina at 30, 35, and 40 mmHg of IOP with maximum IOP in a normal eye (22 mmHg)

IOP (mmHg)	Max. deformation in the retina (mm)	Difference between max. deformation and max. deformation in the normal eye (mm)	Percentage of increased deformation relative to deformation in the normal eye	Max. stress in the retina (Pa)	Difference between max. stress and max. stress in the normal eye (Pa)	Percentage of increased stress relative to stress in the normal eye	Max. strain in the retina	Difference between max. strain and max. strain in the normal eye	Percentage of increased strain relative to strain in the normal eye
30	0.17746	0.02951	19.94 %	5835.4	1280.7	28.12 %	0.29248	0.06367	27.83 %
35	0.17753	0.02958	19.99 %	5850.0	1295.3	28.44 %	0.29321	0.06440	28.14 %
40	0.17754	0.02959	20.00 %	5858.5	1303.8	28.62 %	0.29363	0.06482	28.33 %

normal eye (20.00% increased deformation). In fact, at IOP of 30 mmHg, the slightest deformation, and at IOP of 40 mmHg, the most deformation occurs relative to the normal eye. Also, values for stress and strain are obtained, displayed in Figures 6 and 7, respectively. The maximum stress in the retina in the normal eye is 4554.7 Pa. The maximum stress in the retina at IOP of 30, 35, and 40 mmHg is 5835.4, 5850, and 5858.5 Pa, respectively, which is 1280.7, 1295.3, and 1303.8 Pa higher, respectively, than the normal eye. In fact, with an increase of 36.3%, 59.1%, and 81.8% in IOP, the increase in stress was 28.12%, 28.44%, and 28.62%, respectively. Also, the maximum strain in the retina in the normal eye is 0.22881. The maximum strain in the retina at IOP of 30, 35, and 40 mmHg is 0.29248, 0.29321, and 0.29363, respectively, which are 0.06367, 0.06440, and 0.06482 higher, respectively, than the normal eye. It means, with an increase of 36.3%, 59.1%, and 81.8% in IOP, the increase in strain was 27.83%, 28.14%, and 28.33%, respectively. In all states, maximum stress and maximum strain occurred at the place of maximum deformation, as expected. The amounts of deformation, stress, and

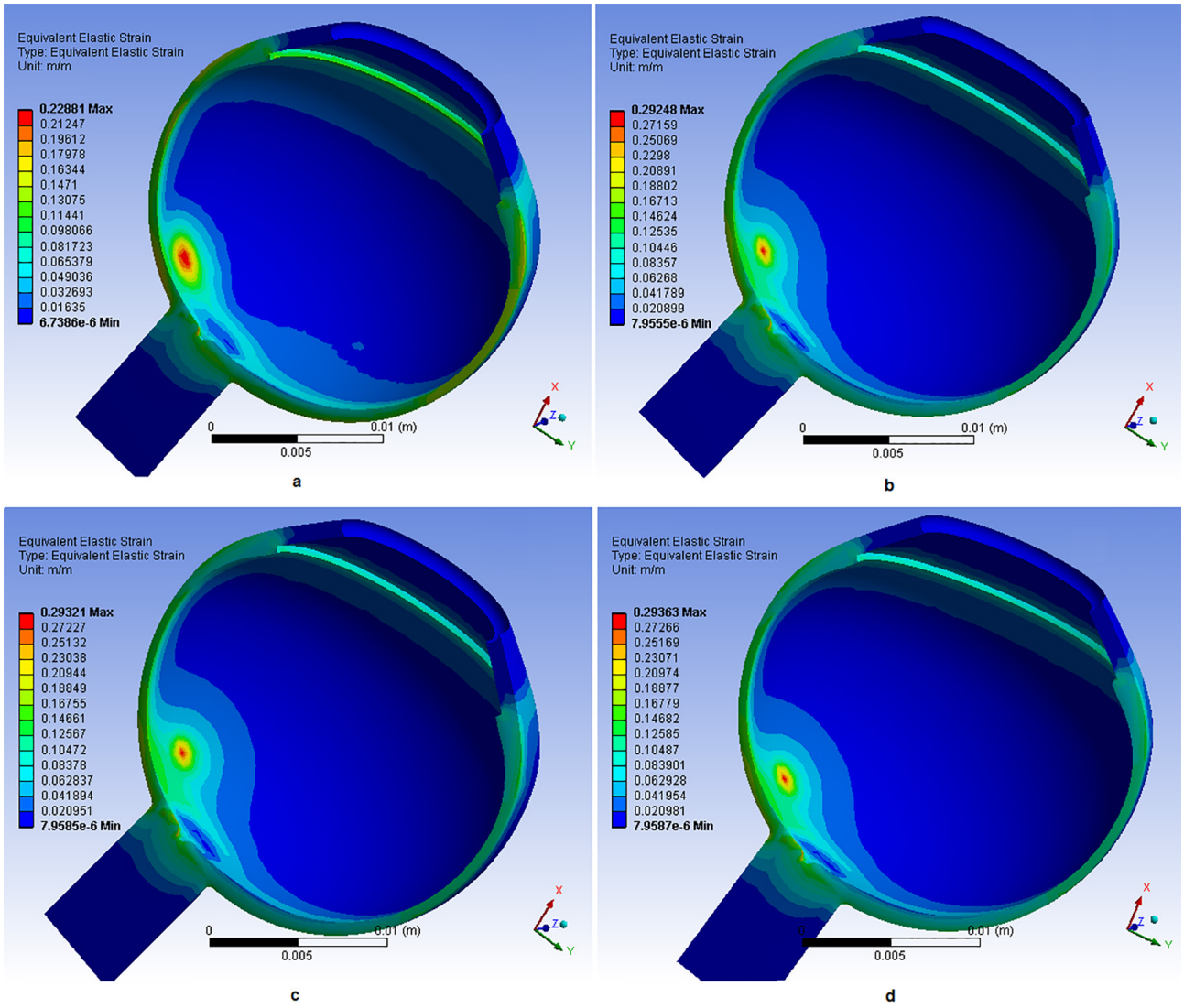

Figure 7-a: Contours of strain in the retina for 22 mmHg of IOP (as a normal eye); **b:** Contours of strain in the retina for 30 mmHg of IOP; **c:** Contours of strain in the retina for 35 mmHg of IOP; **d:** Contours of strain in the retina for 40 mmHg of IOP

Table 5: Comparison of current study with Wang's research [13]

Data	Current study	Wang study
IOP (mmHg)	22	21.13
Minimum strain in the optic disc	3.6%	1.7%
Maximum strain in the optic disc	12%	9.4%
Average strain in the optic disc	7.8%	6.41%

strain relative to the normal eye (22 mmHg of IOP) are specified in Table 4.

To validate the accuracy of the data, the strain at the optic disc was compared with the results of Wang et al. for IOP of 22 mmHg [13]. The difference was 1.39%, as shown in Table 5.

Conclusion

In patients with increased IOP, the amount of deformation in the retina is increased. The increase in deformation is 0.02951, 0.02958, and 0.02959 mm for IOPs of 30, 35, and 40 mmHg, respectively. The maximum deformation occurred near the optic disc in all cases. Furthermore, maximum stress and maximum strain occurred at the place of maximum deformation, as expected. The increase in stress was 1280.7, 1295.3, and 1303.8 Pa and the increase in strain was 0.06367, 0.06440, and 0.06482 for IOPs of 30, 35, and 40 mmHg, respectively. The retina is a very delicate and sensitive member (Young's modulus: 20KPa); most certainly, an increase in stress of about 1300 Pascal will cause irreparable damage to this layer. Therefore, the prevention of glaucoma with an annual ophthalmologist examination is essential.

Conflict of Interest: None declared.

References

1. Bekerman I, Gottlieb P, Vaiman M. Variations in eyeball diameters of the healthy adults. J Ophthalmol 2014; Article ID 503645.
2. Tan CS, Ouyang Y, Ruiz H, Sadda SR. Diurnal variation of choroidal thickness in normal, healthy subjects measured by

spectral domain optical coherence tomography. Invest Ophthalmol Vis Sci 2012; 53: 261-266.
3. Broquet J, Roy S, Mermoud A. Visualization of the aqueous outflow pathway in the glaucoma surgery by finite element model of the eye. Comput Methods Biomech Biomed Engin 2005; 8 (1): 43-44.
4. Akhmanova MA, Domogatsky SP, Evgrafov VY. Computer simulation of hydraulic flows in the human eye. Biophysics 2011; 56 (1): 108-113.
5. Can OF. Exposure of the human eye to wind. Biocybern Biomed Eng 2016; 36 (1): 130-137.
6. Heys JJ, Barocas VH. A boussinesq model of natural convection in the human eye and the formation of Krukenberg's spindle. Ann Biomed Eng 2002; 30 (3): 392-401.
7. Cicekli U. Computational model for heat transfer in the human eye using the finite element method [dissertation]. Agricultural and Mechanical College, Louisiana State Univ.; 2003.
8. Ng EY, Ooi EH. FEM simulation of the eye structure with bio-heat analysis. Comput Methods Programs Biomed 2006; 82 (3): 268-276.
9. Ng EY, Ooi EH. Simulation of aqueous humor hydrodynamics in human eye heat transfer. Comput Biol Med 2008; 38 (2): 252-262.
10. Villamarin A, Roy S, Hasballa R, Vardoulis O, Reymond P, Stergiopulos N. 3D simulation of the aqueous flow in the human eye. Med Eng Phys 2012; 34 (10): 1462-1470.
11. Norman RE, Flanagan JG, Sigal IA, Rausch SMK, Tertinegg I. Finite element modeling of the human sclera: Influence on optic nerve head biomechanics and connections with glaucoma. Exp Eye Res 2011; 93 (1): 4-12.
12. Sigal IA, Flanagan JG, Tertinegg I, Ethier CR. Finite Element Modeling of Optic Nerve Head Biomechanics. Invest Ophthalmol Vis Sci 2004; 45: 4378-4387.
13. Wang X, Beotra MR, Tun TA, Baskaran M, Perera S, Aung T, et al. In vivo 3-dimensional strain mapping confirms large optic nerve head deformations following horizontal eye movements. Invest Ophthalmol Vis Sci 2016; 57: 5825-5833.
14. Tsai JC. High Eye Pressure and Glaucoma. Glaucoma Research Foundation 2015 September. Available from: http://www.glaucoma.org/gleams/high-eye-pressure-and-glaucoma.php
15. Mauro A, Massarotti N, Salahudeen M, Romano MR, Romano V, Nithiarasu P. A generalised porous medium approach to study thermo-fluid dynamics in human eyes. Med Biol Eng Comput 2018; 56 (10): 1823-1839.
16. Thijssen JM, Mol HJM, Timmer MR. Acoustic parameters of ocular tissues. Ultrasound Med Biol 1985; 11 (1): 157-161.
17. Donati S, Caprani SM, Airaghi G, Vinciguerra R, Bartalena L, Testa F, et al. Vitreous substitutes: The present and the future. Biomed Res Int 2014; Article ID 351804.
18. Phillips JR, McBrien NA. Form deprivation myopia: elastic properties of sclera. Ophthalmic Physiol Opt 1995; 15 (5): 357-362.
19. Battaglioli JL, Kamm RD. Measurements of the compressive properties of scleral tissue. Investigative Ophthalmology & Visual Science. Invest. Ophthalmol Vis Sci 1984; 25 (1): 59-65.
20. Friberg TR, Lace JW. A comparison of the elastic properties of human choroid and sclera. Exp Eye Res 1988; 47 (3): 429-436.
21. Jones IL, Warner M, Stevens JD. Mathematical modelling of the elastic properties of retina: a determination of Young's modulus. Eye 1992; 556-559.
22. Franze K, Francke M, Gunter K, Christ AF, Korber N, Reichenbach A, et al. Spatial mapping of the mechanical properties of the living retina using scanning force microscopy. Soft Matter 2011; 7 (7): 3025-3652.
23. Heys J, Barocas VH. Mechanical characterization of the bovine iris. J Biomech 1999; 32 (9): 999-1003.
24. Fisher RF. The elastic constants of the human lens. J Physiol 1971; 212 (1): 147-180.
25. Bailey ST, Twa MD, Gump JC, Venkiteshwar M, Bullimore MA, Sooryakumar R. Light scattering study of the normal human eye lens: Elastic properties and age dependence. IEEE Trans Biomed Eng 2010; 57 (12): 2910-2917.
26. Uchio E, Ohno S, Kudoh J, Aoki K, Kisielewicz LT. Simulation model of an eyeball based on finite element analysis on a supercomputer. British Journal of Ophthalmology 1999; 83 (10): 1106-1111.